On the Oxidation of α-Fe and ε-Fe2N1-z

Jutte, Robin H.; Kooi, Bart J.; Somers, Marcel A.J.; Mittemeijer, Eric J.

Published in:
Oxidation of Metals

DOI:
10.1007/BF01675263

Oxidation of Metals, Vol. 48, Nos. 1/2, 1997

On the Oxidation of α-Fe and ε-Fe_2N_{1-z}: I. Oxidation Kinetics and Microstructural Evolution of the Oxide and Nitride Layers

Robin H. Jutte,† Bart J. Kooi,‡ Marcel A. J. Somers,* and Eric J. Mittemeijer*

Received January 25, 1996; revised November 18, 1996

The oxidation of α-Fe and ε-Fe_2N_{1-z} at 573 K and 673 K in O_2 at 1 atm was investigated by thermogravimetrical analysis, X-ray diffraction, light-optical microscopy, scanning electron microscopy and electron probe X-ray microanalysis. Upon oxidation at 573 K and 673 K, on α-Fe initially α-Fe_2O_3 develops, whereas on ε-Fe_2N_{1-z} initially Fe_3O_4 develops. In an early stage of oxidation the oxidation rate of ε-Fe_2N_{1-z} appears to be much larger than of α-Fe. This can be attributed largely to an effective surface area available for oxygen uptake, which is much larger for ε-Fe_2N_{1-z} than for α-Fe due to the porous structure of ε-Fe_2N_{1-z} as prepared by gaseous nitriding of iron. The development of a magnetite layer in-between the hematite layer and the α-Fe substrate, at a later stage of oxidation, enhances layer-growth kinetics. After 100 min oxidation at 673 K the (parabolic) oxidation rates for α-Fe and ε-Fe_2N_{1-z} become about equal, indicating that on both substrates the oxide growth is controlled by the same rate limiting step which is attributed to short-circuit diffusion of iron cations. Oxidizing ε-Fe_2N_{1-z} increases the nitrogen concentration in the remaining ε-iron nitride, because the outward flux of iron cations, necessary for oxide growth, leads to an accumulation of nitrogen atoms left behind.

KEY WORDS: oxidation; kinetics; iron; iron-nitride.

*Laboratory of Materials Science, Delft University of Technology, Rotterdamseweg 137, NL-2628 AL Delft, The Netherlands.
†Present address: Directorate-General of Public Works and Water Management, Road and Hydraulic Engineering Division, PO Box 5044, NL-2600 GA Delft, The Netherlands.
‡Present address: Department of Applied Physics, Materials Science Center, University of Groningen, Nijenborgh 4, NL-9747 AW Groningen, The Netherlands.

0030-770X/97/0800-0087$12.50/0

Table I. Compositions (in ppm by mass) of Types of Iron Used in Oxidation and Nitriding (+oxidation) Treatments

Fe-type	C	N	O	S	Al	Si	Ti	Cr	Mn	Ni	V	W	Fe
Ferrovac-E	44	10	101	30	16	—	4	6	4	124	<3	<3	balance
J&M	8	17	30	<10	<1	7	<10	13	<1	<1	7	<10	balance
Refined	27	138	111	15	<10	—	<10	20	6	77	10	87	balance

INTRODUCTION

The resistance against atmospheric corrosion of a ferritic workpiece can be improved by application of a compound layer at the surface[1,2] composed of the iron-nitrides ε-$Fe_2(N, C)_{1-z}$ and γ'-$Fe_4(N, C)_{1-x}$, as brought about by a nitriding (nitrocarburizing) treatment.[3] A further significant enhancement of the atmospheric corrosion resistance is realized by transformation of the surface-adjacent part of the iron-nitride compound layer into iron oxide(s) by an oxidation treatment.[4,5] Several commercial processes combining the nitriding (nitrocarburizing) and oxidation treatments have been developed.[6]

A thorough understanding of the mechanisms responsible for the improvement of the corrosion resistance is lacking. Hence, optimization of the corrosion properties on the basis of insight rather than by empirical methods is not (yet) possible. Knowledge about the similarities of and differences between the oxidation of ferrite and of iron nitride, in particular with respect to the evolutions of the constitution and the residual strains occurring in the oxide layer, may lead to understanding of the improvement of the corrosion properties by development of an oxide layer on iron nitride.

In previous papers, the present authors reported on the oxidation of γ'-Fe_4N_{1-x} layers at 603 K and 673 K in O_2 at 1 atm and showed that during oxidation ε-Fe_2N_{1-z} nucleated in-between the parent γ'-Fe_4N_{1-x} layer and the Fe_3O_4/α-Fe_2O_3 (magnetite/hematite) overlayer formed.[7,8] A comparative analysis of the oxidation kinetics of α-Fe and ε-Fe_2N_{1-z}, the iron-nitride phase usually occurring at the surface of the compound layer, and of the microstructural evolution in the oxide and nitride layers is the subject of this paper. The development of residual strains in the oxide layer is discussed in the following paper.[9]

EXPERIMENTAL PROCEDURES

Nitriding and Oxidizing

Direct oxidation of α-Fe was performed for three types of α-Fe, which will be referred to as Ferrovac-E, J&M (Johnson & Matthey) and Refined (for compositions see Table I). The samples were used in a recrystallized

condition which was obtained by annealing 70% cold-rolled iron at 923 K for 30 min in pure H_2. The standard surface preparation of the α-Fe sample after recrystallization before oxidation involved: (1) grinding with paper of grit P1200; (2) chemical polishing in Kawamura's reagent (80 vol.% H_2O_2, 15 vol.% destilled water, 5 vol.% HF) for $2\frac{1}{2}$ min.; (3) etching in 1% Nital (1% HNO_3 in ethanol) for 30 sec; (4) ultrasonical cleaning in 2-propanol, except when indicated otherwise. To investigate the influence of the treatment of α-Fe prior to oxidation on the constitution of the oxide layer a separate experiment involving another specimen pretreatment was performed. In this experiment 70% cold-rolled α-Fe (Refined) was treated according to the standard surface-preparation treatment indicated above and additionally, prior to oxidation, was annealed (recrystallized) at 923 K for 30 min in pure H_2.

The nitride layers on top of α-Fe substrates were prepared by nitriding 70% cold-rolled α-Fe. Before nitriding, preparation steps identical to those prior to direct oxidation of pure iron and described above were carried out. Nitriding of cold rolled Ferrovac-E was performed at 838 K for $3\frac{1}{2}$ hr (unless otherwise indicated; cf. Fig. 1) in a gas mixture composed of 55 vol.% NH_3 and 45 vol.% H_2 to obtain a surface layer of ε-Fe_2N_{1-z} of about 13-μm thickness on top of a γ'-Fe_4N_{1-x} sublayer of about 4-μm thickness. The ε-sublayer showed a limited amount of porosity as a consequence of the nitriding treatment. For discussion of the origin of this porosity, see Ref. 10 and morphology section. For some specific cases α-Fe of type Refined was used. A nitride layer on cold-rolled Refined iron, as produced under the same nitriding conditions as for Ferrovac-E, had a thinner ε-Fe_2N_{1-z} sublayer (4 μm) on top of a thicker γ'-Fe_4N_{1-x} sublayer (8 μm). Therefore, the nitriding conditions for cold-rolled Refined iron were modified to either (i) $3\frac{1}{2}$ hr at 838 K in a gas mixture composed of 69 vol.% NH_3 and 31 vol.% H_2 or (ii) 3 hr at 838 K in a gas mixture composed of 75.8 vol.% NH_3 and 24.2 vol.% H_2. Nitriding conditions (i) resulted in a practically pore-free epsilon layer of thickness 10 μm, which will be referred to as "dense" ε-Fe_2N_{1-z}; nitriding conditions (ii) resulted in an epsilon sublayer, of thickness 13 μm, slightly more porous than as obtained with the standard nitriding treatment of Ferrovac-E (see above) and this layer will be referred to as "porous" ε-Fe_2N_{1-z}. The ε layer obtained with the standard nitriding treatment applied to Ferrovac-E, which is slightly porous, will be referred to without the designation "dense" or "porous".

Experimental details of gas purification, gas-flow control and nitriding equipment have been given in Ref. 10. The gas flow in the nitriding furnace corresponded to a linear gas velocity of 5.8 mm/sec. After nitriding and before oxidizing no additional preparation of the nitrided surface was carried out.

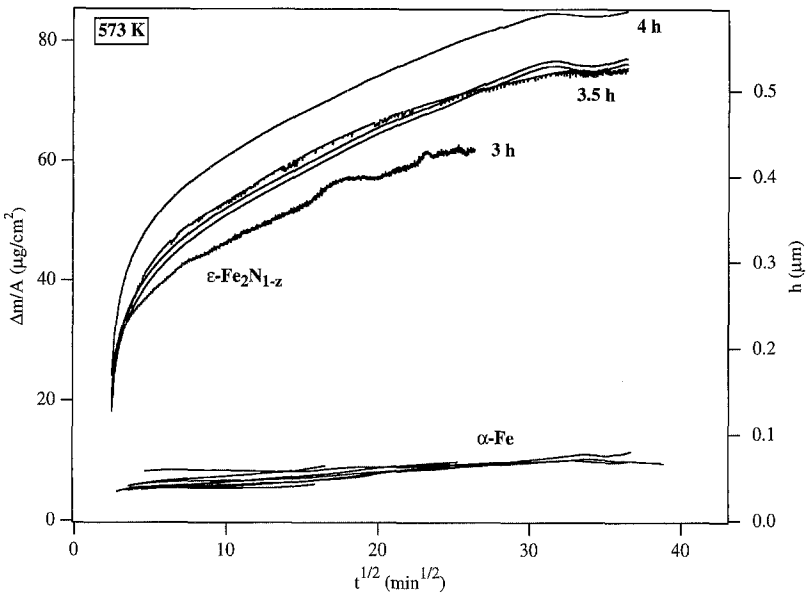

Fig. 1. Mass increase Δm per unit of surface A, $\Delta m/A$, of α-Fe (J&M and Refined) and ε-Fe_2N_{1-z} samples due to oxidation at 573 K in O_2 at 1 atm as a function of the square root of the oxidation time, t. The corresponding oxide-overlayer thickness, h, that would apply if a single-phase Fe_3O_4 layer of uniform thickness would have formed is indicated on the right-hand ordinate. The ε-Fe_2N_{1-z} samples were obtained by nitriding of α-Fe (Ferrovac-E) in an NH_3/H_2 gas mixture of 55 vol.% NH_3 and 45 vol.% H_2 at 838 K using several nitriding times: 3, $3\frac{1}{2}$ (the standard treatment; see Nitriding and Oxidizing section) and 4 hr as indicated in the figure.

Oxidation was performed at 573 K or at 673 K at 1 atm in high purity O_2 ($CH_4 < 0.5$ ppm, $CO + CO_2 < 0.5$ ppm, $H_2O < 1$ ppm, N_2 + inert gases < 7 ppm, $H_2 < 1$ ppm). The oxidation equipment for investigation of the oxidation kinetics is discussed in the following section. Samples for X-ray diffraction phase identification and residual-strain determination[9] were oxidized in a separate horizontal quartz-tube furnace (temperature control within 1 K) for selected times in the same high-purity O_2.

Thermogravimetric Analysis (TGA)

The kinetics of the oxidation of α-Fe and ε-Fe_2N_{1-z} were investigated by Thermogravimetric Analysis (TGA) in a Netzsch TG439 instrument. This apparatus consists of a symmetrical balance with separate furnaces for the sample and the reference. It was verified that the furnaces did not exert an electromagnetic force on the ferromagnetic specimens, which would hinder an accurate determination of the mass changes from the weight

changes recorded during oxidation. The sensitivity of the balance is 0.1 μg and the drift of the instrument was below 2 μg/hr. Different buoyancy effects for sample and reference were corrected for. Samples were heated at a rate of 50 K/min up to the oxidation temperature desired; temperature control was within 0.1 K. During oxidation an O_2 gas-flow velocity of 0.65 mm/sec was maintained in the thermobalance.

Light Microscopical (LMA) and Scanning Electron Microscopical (SEM) Analysis

A Neophot 30 (Zeiss, Jena) light-optical microscope was used for Light Microscopical Analysis (LMA) of the surfaces and cross-sections of the samples. In order to prevent damaging of the oxide layers during the preparation of cross-sections, first a thin layer of Ag was deposited by evaporation onto the specimen and then a Ni-support layer was deposited electrolytically onto the specimen. Samples for LMA were polished, using, as the final step, 1/4-μm diamond paste, and thereafter etched in 1% Nital.

A Jeol JSM 840 scanning electron microscope (SEM) was used to study fracture surfaces of oxidized α-Fe and ε-Fe_2N_{1-z}. Fracture surfaces were obtained by sawing a notch on one side of the 0.35-mm thick specimens oxidized in the thermobalance and brittle fracturing the specimens, at boiling N_2 temperature (77 K).

X-Ray Diffraction (XRD) Phase Identification

X-Ray Diffraction (XRD) experiments were performed with Siemens diffractometers of the types F – ω and D-500, which were used with a line focus and were equipped with a curved graphite monochromator in the diffracted beam. Measurements were performed applying the Bragg-Brentano geometry and Cu K_α radiation. The diffraction-angle range scanned was 22.5–80 °2Θ with a step size of 0.05 or 0.1 °2Θ.

All nitrided and oxidized iron samples examined by XRD analysis were of the Refined type (see Nitriding and Oxidizing section and Table I).

Electron Probe X-Ray Micro Analysis (EPMA)

A Jeol JXA 733 electron probe X-ray microanalyzer equipped with four wavelength-dispersive spectrometers and an energy-dispersive system, coupled with Tracor Northern TN 5500 and TN 5600 systems for instrument control, data acquisition and data analysis, was used for determination of the N, O, and Fe concentrations on cross sections of the samples. A focused electron beam for generation of the characteristic X-rays was operated at 10 kV. The intensities of N K_α, O K_α and Fe K_α radiations of the samples

investigated were divided by those of γ'-Fe_4N_{1-x} ($x=0.024$), SiO_2, and Fe standards, respectively. Concentration values were calculated from these intensity ratios by applying the modified $\Phi(\rho z)$ approach.[11] Carbon contamination at the measurement location was removed prior to measurement of the X-ray intensities by blowing an air jet along the exposed surface of the specimen cross section for at least 30 sec, while the electron beam was on. The nitrogen and iron contents as measured for the nitride layer were corrected for the presence of oxygen (about 2 at.% O; predominantly due to oxidation of the exposed surface by the air jet): from the measured oxygen content on the nitrides the corresponding iron content was obtained, assuming that all oxygen was present as Fe_3O_4 at the exposed surface and that the nitride was composed of only iron and nitrogen. The corresponding iron content was subtracted from the measured iron content and the sum of the nitrogen content and the remaining iron content was normalized to 100%. Also the presence of oxygen from oxide in the pores was corrected for in this way.

The composition-depth profiles of a nitrided sample and of a sample additionally oxidized at 673 K for 16 hr in O_2 were determined in cross sections along straight lines making an angle of about 13° with the nitride/ferrite interface.

RESULTS AND INTERPRETATION

Mass Increase; Oxidation Kinetics

The mass increase of α-Fe and ε-Fe_2N_{1-z} samples due to oxygen uptake by oxidation at 573 K and 673 K is given as a function of the square root of the oxidation time in Figs. 1 and 2, respectively. The corresponding oxide overlayer thickness, that would apply if a single-phase Fe_3O_4 layer of uniform thickness would have formed, is indicated on the right-hand ordinate. If single-phase α-Fe_2O_3 layers would have formed, the same ordinate applies within good approximation.

Clearly, the oxygen uptakes of α-Fe and ε-Fe_2N_{1-z} differ vastly. At 573 K the oxygen-uptake for α-Fe is almost negligible as compared to that for ε-Fe_2N_{1-z}. Also at 673 K the oxygen uptake for α-Fe is considerably smaller than that for ε-Fe_2N_{1-z}. After about 50 min of oxidation at 673 K the oxygen-uptake rates for α-Fe and ε-Fe_2N_{1-z} become approximately equal, suggesting that the rate-determining step in the oxidation kinetics is the same for both substrates. After about 100 min of oxidation at 673 K the oxygen uptakes for α-Fe and ε-Fe_2N_{1-z} depend approximately linearly on the square root of the oxidation time, indicating parabolic layer-growth kinetics.

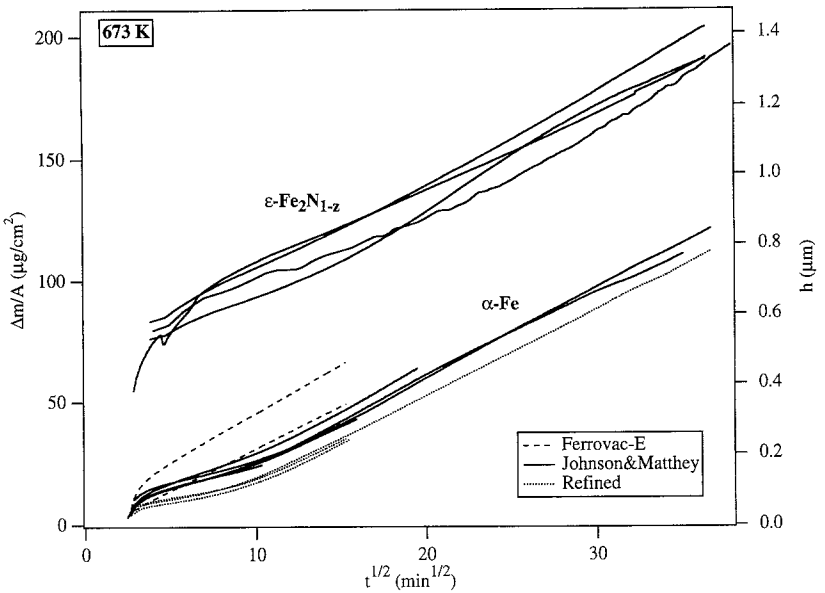

Fig. 2. Mass increase per unit of surface area, $\Delta m/A$, of α-Fe and ε-Fe_2N_{1-z} samples (prepared by the standard nitriding treatment; see Nitriding and Oxidizing section) due to oxidation at 673 K in O_2 at 1 atm as a function of the square root of the oxidation time, t. The corresponding oxide-overlayer thickness, h, that would apply if a single-phase Fe_3O_4 layer of uniform thickness would have formed is indicated on the right-hand ordinate. Three different types of α-Fe were used, which differ in impurity level (see Table I).

The nitriding time for manufacturing the ε-Fe_2N_{1-z} surface layer has a distinct effect on the total oxygen uptake (Fig. 1). The longer the nitriding time, the larger is the subsequent oxygen uptake. This difference in oxygen uptake is predominantly due to differences in oxygen uptake during the first 20 min of oxidation.

The impurity content of the α-Fe substrate (cf. Table I) influences the oxygen-uptake rate at 673 K until an oxidation time of about 100 min, after which the oxidation kinetics become approximately parabolic (Fig. 2 and see above).

Morphology

Blisters were observed to have formed at several locations of the oxidized α-Fe surfaces, irrespective of the type of iron or the oxidation temperature used. Blisters observed at room temperature after oxidation at 673 K for times ranging from about 10 to 225 min have similar appearances as those observed upon oxidation at 573 K for times ranging from about 500

to 1320 min. For iron with a relatively low impurity content (J&M) the blisters that had formed after relatively short oxidation times expanded over an entire ferrite-grain and in most cases stopped at a ferrite-grain boundary (see micrograph in Fig. 3a). For iron with a relatively high impurity content (Refined) blisters were observed to be pinned within ferrite grains at small inclusions in the surface (see micrograph in Fig. 3b).

The morphology of the blisters evolved from the type shown in Fig. 3, for the relatively short oxidation times, to patterns of wrinkles on the grain surfaces on prolonged oxidation (Fig. 4).

Blister formation on oxidized α-Fe substrates may indicate poor adherence of the oxide layer to the ferrite substrate. An SEM view of fractured α-Fe (J&M) oxidized at 673 K for 1320 min shows an oxide overlayer that appears to be detached from the substrate (Fig. 5). Two regions can be discerned within the oxide layer: a featureless zone adjacent to the substrate and a fine-grain zone adjacent to the surface. These regions may correspond to the two oxide phases Fe_3O_4 and α-Fe_2O_3, respectively (see XRD results presented in Oxide-Phase Development section).

Blistering of oxide layers was not observed for the oxidized ε-Fe_2N_{1-z} substrates (cf. Figs. 6 and 7). This absence suggests a better adherence of iron oxide on ε-Fe_2N_{1-z} than on ferrite.

A micrograph of a cross-section of ε-Fe_2N_{1-z} oxidized at 573 K for 1320 min is shown in Fig. 6. Both the porous ε-Fe_2N_{1-z} layer (about 12.5 μm thick) and the intermediate layer of γ'-Fe_4N_{1-x} (about 3-μm thick) on top of the α-Fe substrate can be observed clearly. The very thin oxide layer, at the location of the dark region between the ε-Fe_2N_{1-z} layer and the Ni support layer, cannot be observed in detail. The porosity in the ε-Fe_2N_{1-z} layer is limited to grain boundaries (see Ref. 10 for a discussion about porosity in Fe–N phases). Precipitates of γ'-Fe_4N_{1-x} are present in the ε-Fe_2N_{1-z} layer at some distance from the surface (indicated by arrows). Fine precipitates of, most likely, α-Fe[7] are present in the γ'-Fe_4N_{1-x} layer, particularly in the part adjacent to the α-Fe substrate (Fig. 6). An SEM view of fractured ε-Fe_2N_{1-z} oxidized at 573 K for 1320 min shows an oxide layer with a thickness of about 0.3 to 1 μm on top of the porous ε-Fe_2N_{1-z} (Fig. 7). A good adherence of the oxide layer is observed (cf. Fig. 5). Close inspection of the edges of the pores reveals that oxidation has occurred inside the ε-Fe_2N_{1-z} layer down to a depth of about 5 μm, which is apparently the depth range over which the pores are in open connection with the outer oxidizing atmosphere.

An SEM view of fractured ε-Fe_2N_{1-z} oxidized at 673 K for 1320 min shows two (distinct) regions in the oxide layer (Fig. 8): a coarse grained zone close to the nitride layer and a fine grain zone close to the surface. These regions may correspond to the two oxide phases Fe_3O_4 and α-Fe_2O_3,

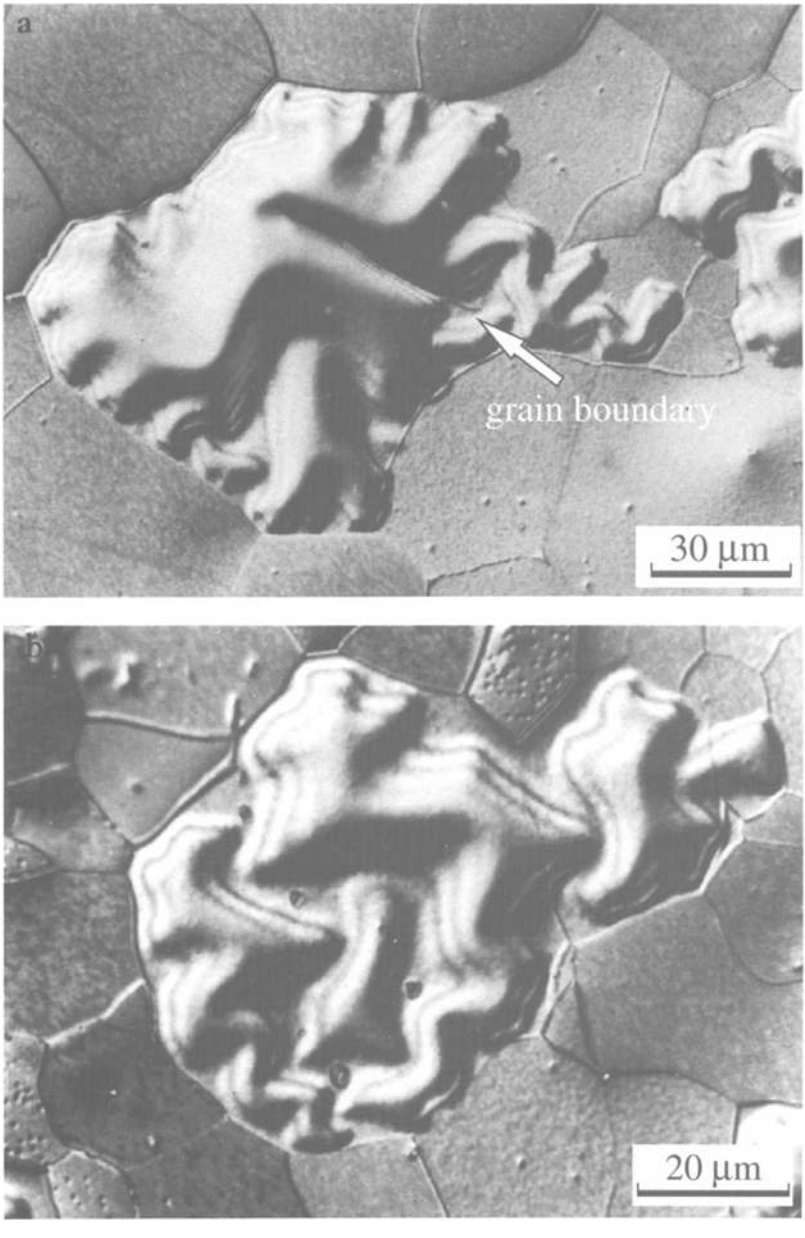

Fig. 3. (a) Micrograph (bright field, monochromatic light: 546 nm) of the surface of α-Fe (J&M) oxidized at 673 K for 10 min. The oxide blister extends over two ferrite grains. Arrow indicates location of grain boundary between the two grains. (b) Micrograph (bright field, monochromatic light: 546 nm) of the surface of α-Fe (Refined) oxidized at 673 K for 10 min. The oxide blister is pinned at small inclusions in the iron.

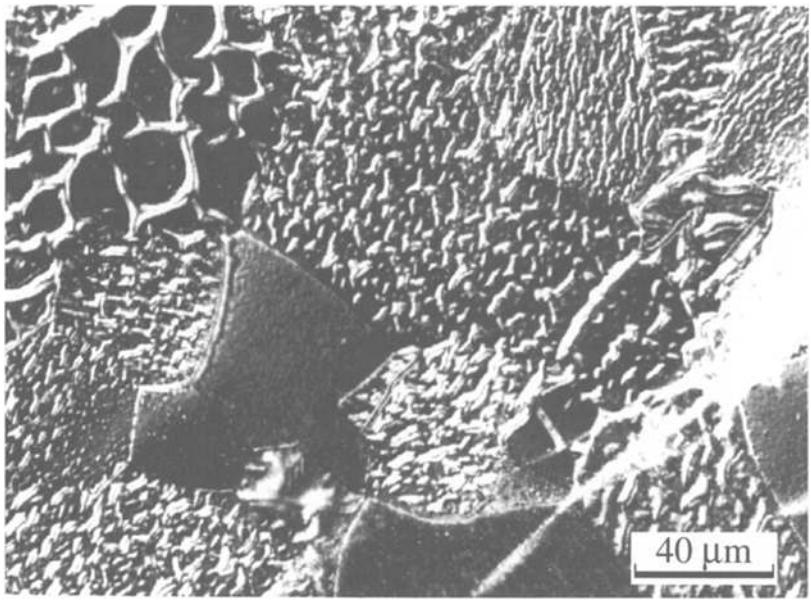

Fig. 4. Micrograph (differential interference contrast) of the surface of α-Fe (J&M) oxidized at 673 K for 100 min showing regular patterns of a wrinkled oxide overlayer on the surface of the various grains of the α-Fe substrate.

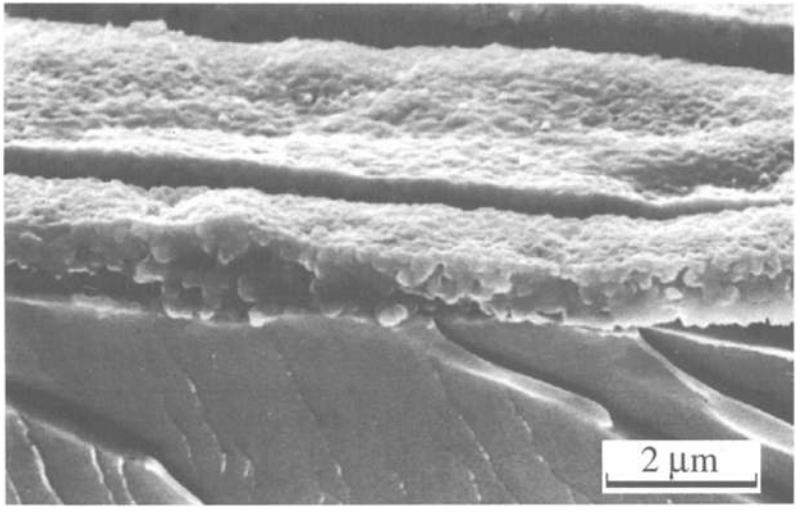

Fig. 5. SEM view of fractured α-Fe (J&M) oxidized at 673 K for 1320 min, showing a cross sectional view of an oxide overlayer with an almost uniform thickness of about 1 μm. Poor adherence of the oxide layer to the ferrite substrate can be observed (cf. Fig. 7).

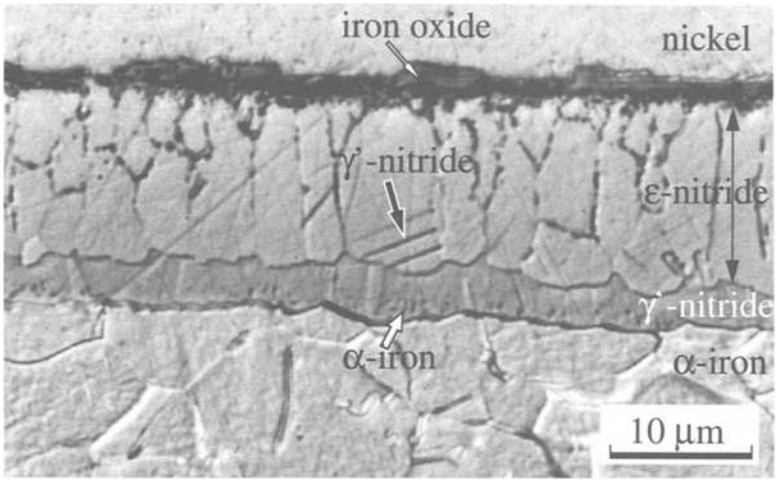

Fig. 6. Micrograph (differential interference contrast) of a cross-section of ε-Fe_2N_{1-z} oxidized at 573 K for 1320 min. The porous ε-Fe_2N_{1-z} layer, of about 12.5 μm thick, on top of the α-Fe substrate with an intermediate layer of γ'-Fe_4N_{1-x}, of about 3 μm thick, can be observed clearly. The oxide, in the dark region between the ε-Fe_2N_{1-z} layer and the Ni support layer, cannot be observed in detail. Plate precipitates of γ'-Fe_4N_{1-x} are present in the ε-Fe_2N_{1-z} layer at some distance from the surface (see black arrow). Fine precipitates of, most likely, α-Fe[7] are present in the γ'-Fe_4N_{1-x} layer, particularly in the part adjacent to the α-Fe substrate (see white arrow).

respectively (see XRD results presented in Oxide Phase Development section). A porous region in ε-Fe_2N_{1-z} can be discerned in Fig. 8 at the interface of the oxide layer and the ε-nitride layer, while the oxide layer is well adhered to the nitride layer.

Oxide-Phase Development

For the oxidation of α-Fe (Refined) at 573 K the evolutions of the magnetite (M; Fe_3O_4) and the hematite (H; α-Fe_2O_3) diffraction-line profiles

Table II. Mass Increase per Unit Surface Area, $\Delta m/A$, for α-Fe (Refined) Oxidized at 573 K in O_2 at 1 atm for the Times Indicated, After the Standard Pretreatment With or Without Additional Annealing in H_2. Corresponding Diffractograms Are Provided in Fig. 9a

Oxidation time (min)	$\Delta m/A$ (μg/cm2)	
	standard	H_2 anneal
16	4.1	4.7
100	5.5	9.0
1320	6.5	25.8

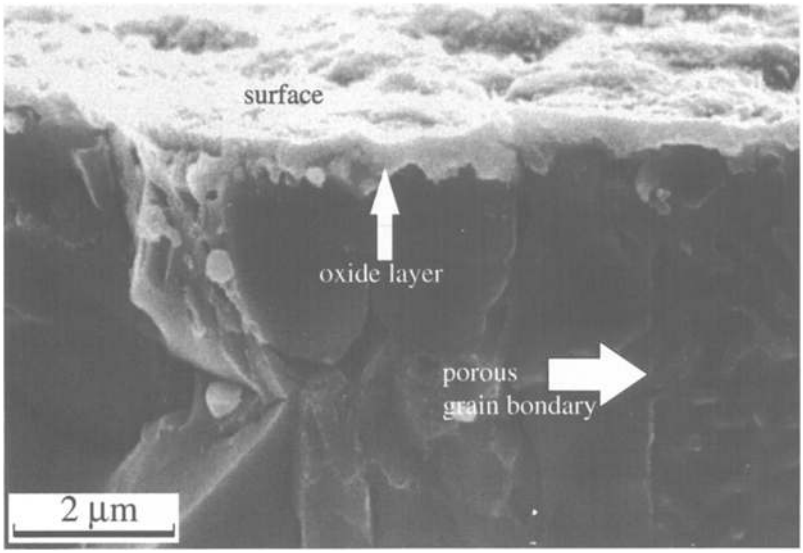

Fig. 7. SEM view of fractured ε-Fe_2N_{1-z} oxidized at 573 K for 1320 min showing a cross-sectional view of an oxide overlayer with a thickness of about 0.3 to 1 μm on top of the porous ε-Fe_2N_{1-z}. Good adherence of the oxide layer is indicated by the micrograph (cf. Fig. 5). Arrow indicates location where porous grain boundary is viewed face on.

are presented in Fig. 9a. The solid lines refer to oxidation of α-Fe that has been subjected to the standard pretreatment and the dashed lines refer to oxidation of α-Fe that has been recrystallized (H_2 annealed) after the standard sample preparation before oxidation (see Nitriding and Oxidizing section). The corresponding amounts of oxygen taken up by the samples have been given in Table II. After 16 min of oxidation at 573 K only α-Fe_2O_3 was present on α-Fe. After 100 min of oxidation α-Fe_2O_3 was still the only phase observable on the standard pretreated α-Fe sample, whereas on the H_2-annealed α-Fe sample a substantial amount of Fe_3O_4 had developed. After 1320 min of oxidation the presence of Fe_3O_4 on H_2-annealed α-Fe is dominant, while on the standard pretreated α-Fe about the same amount of Fe_3O_4 developed as on the H_2-annealed α-Fe after 100 min of oxidation.[§] It is concluded that on oxidation of α-Fe at 573 K first α-Fe_2O_3 develops before Fe_3O_4 occurs and that the time after which Fe_3O_4 develops depends on the preparation conditions of the α-Fe sample.

For the oxidation of "porous" ε-Fe_2N_{1-z} at 573 K the evolutions of the Fe_3O_4 and the α-Fe_2O_3 diffraction-line profiles are presented in Fig. 9b.

§The qualitative discussion in this paragraph ignores effects due to absorption of the X-rays, which is justified, because the information depth[27] in the XRD experiments is much larger than the total oxide-overlayer thickness.

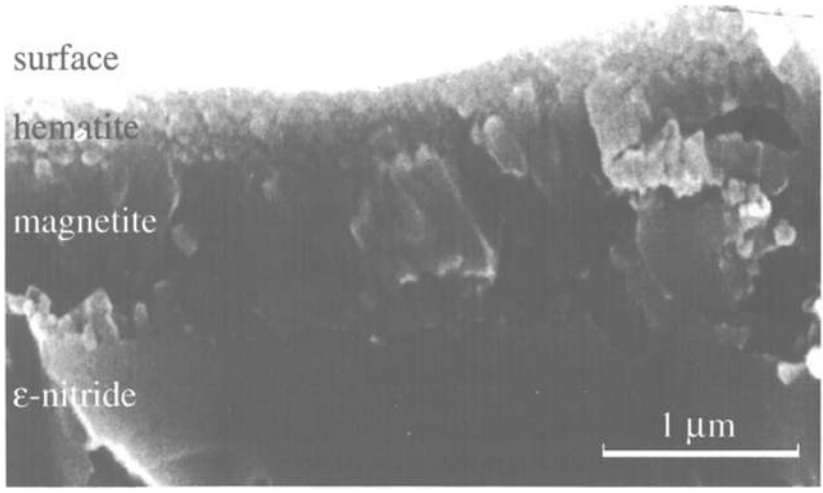

Fig. 8. SEM view of fractured ε-Fe_2N_{1-z} oxidized at 673 K for 1320 min showing a cross-sectional view of two (distinct) regions in the oxide layer: a coarse-grain zone close to the nitride layer and a fine-grain zone close to the surface. These regions probably correspond to the two oxide phases Fe_3O_4 and α-Fe_2O_3, respectively. A porous region in ε-Fe_2N_{1-z} at the nitride/oxide interface can be discerned.

Contrary to the observations for α-Fe, on ε-Fe_2N_{1-z} only Fe_3O_4 was observed after 16 min of oxidation at 573 K. Evidently, ε-Fe_2N_{1-z} promotes the immediate nucleation of Fe_3O_4 rather than of α-Fe_2O_3 on its surfaces. At a later stage of oxidation α-Fe_2O_3 was also observed. After prolonged oxidation at 573 K the amounts of α-Fe_2O_3 relative to Fe_3O_4 are similar for ε-Fe_2N_{1-z} and H_2-annealed α-Fe.

For the oxidation of α-Fe (Refined) at 673 K the evolutions of the Fe_3O_4 and the α-Fe_2O_3 diffraction-line profiles are presented in Fig. 10a. As for oxidation at 573 K, oxidation of α-Fe at 673 K gives rise to the initially preferred formation of α-Fe_2O_3. However, at 673 K already after 16 min of oxidation some Fe_3O_4 had developed. For oxidation times ranging from about 16 to 100 min mainly growth of Fe_3O_4 was observed.

For the oxidation of "porous" ε-Fe_2N_{1-z} at 673 K the evolutions of the Fe_3O_4 and the α-Fe_2O_3 diffraction-line profiles are presented in Fig. 10b. After 16 min of oxidation at 673 K both Fe_3O_4 and α-Fe_2O_3 were present. On prolonged oxidation α-Fe_2O_3 was observed to be the dominantly growing phase.

Concentration-Depth Profiles

Two samples were investigated with EPMA. One sample was nitrided according to the standard procedure for formation of the ε-Fe_2N_{1-z} surface

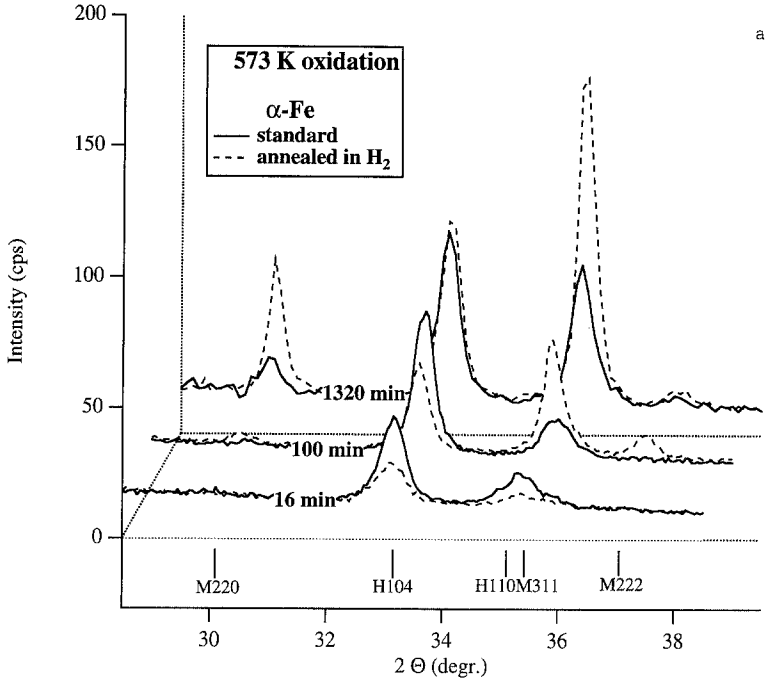

Fig. 9. (a) Diffractograms (CuK_α radiation) showing the magnetite (M; Fe_3O_4) {220}, {311} and {222} line profiles and the hematite (H; α-Fe_2O_3) {104} and {110} line profiles for α-Fe (Refined) samples oxidized during 16, 100, and 1320 min at 573 K in O_2 at 1 atm. Two different surface pretreatments of the α-Fe samples prior to oxidation were used: standard pretreatment (solid lines) or standard pretreatment with additional annealing in H_2 (dashed lines). (b) Diffractograms (CuK_α radiation) showing the magnetite (M; Fe_3O_4) {220}, {311}, and {222} line profiles and the hematite (H; α-Fe_2O_3) {104} and {110} line profiles for "porous" ε-Fe_2N_{1-z} samples oxidized during 16 and 1320 min at 573 K in O_2 at 1 atm. The 2Θ positions of the reflections pertaining to ε nitride (E) with a nitrogen content of 25 at.% N (Fe_3N) are indicated with {*hkl*} indexing relative to the sublattice of nitrogen atoms,[26] using the lattice parameter dependences given in Ref. 28.

layer and the other sample was identically nitrided and subsequently oxidized for 16 hr at 673 K. Composition-depth profiles as determined in cross sections of these samples by EPMA are given in Fig. 11. The presentation of the concentration-depth profiles is such that the nitride-layer/ferrite-substrate interface for the nitrided and oxidized sample is taken at the same depth location as for the nitrided sample.

A constant oxygen amount of 2 at.%, predominantly due to oxidation by the air jet used for the removal of carbon contamination (see Electron Probe X-Ray Micro Analysis (EPMA) section), was subtracted from the O profiles in Fig. 11. For the nitrided and oxidized sample the oxygen content

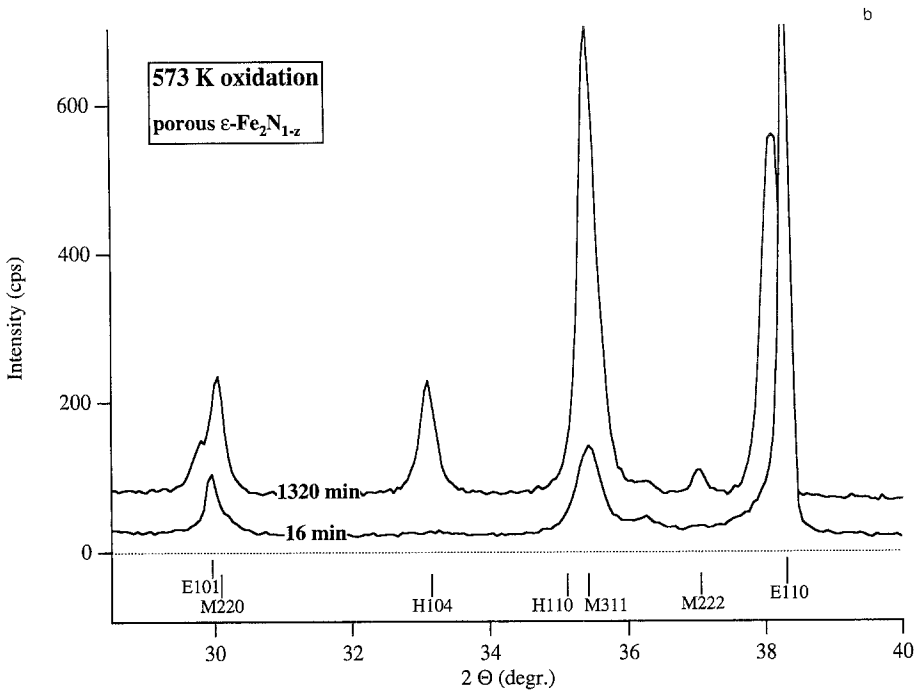

Fig. 9. Continued.

in the oxide layer was between that of Fe_3O_4 (57 at.% O) and of α-Fe_2O_3 (60 at.% O). The depth range where the nitrogen content varies from about 24 to about 29 at.% N is taken as coinciding with the ε-Fe_2N_{1-z} layer; the plateau where the nitrogen content is about 20 at.% is taken as corresponding with the γ'-Fe_4N_{1-x} layer.

The large fluctuations of the nitrogen content close to the ε/γ' interface observed for the oxidized sample are attributed to the presence of γ'-phase in the ε-phase that precipitates during the oxidation treatment (see black arrow in Fig. 6). Further, upon oxidation the nitrogen content in the ε-sublayer beneath the oxide layer has increased.

DISCUSSION

Oxidation Kinetics of α-Fe

According to the Fe–O phase diagram[12] it is expected on oxidation of α-Fe at 573 K and 673 K that, provided the oxygen partial pressure in the oxidizing gas is sufficiently high to allow the formation of hematite (at

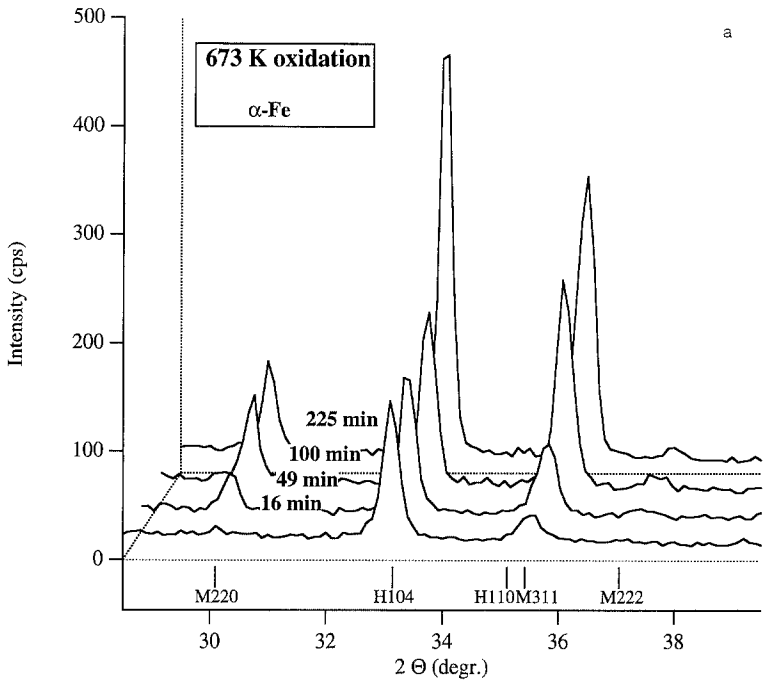

Fig. 10. (a) Diffractograms (CuK_α radiation) showing the magnetite (M; Fe_3O_4) {220}, {311} and {222} line profiles and the hematite (H; α-Fe_2O_3) {104}, {110}, and {113} line profiles for α-Fe (Refined) samples oxidized during 16, 49, 100, and 225 min at 673 K in O_2 at 1 atm. (b) Diffractograms (CuK_α radiation) showing the magnetite (M; Fe_3O_4) {220}, {311}, and {222} line profiles and the hematite (H; α-Fe_2O_3) {104} and {110} line profiles for "porous" ε-Fe_2N_{1-z} samples oxidized during 16, 49, 100, 225 and 1320 min at 673 K in O_2 at 1 atm. The 2Θ positions of the reflections pertaining to ε nitride (E) with a nitrogen content of 29 at.% N are indicated with {*hkl*} indexing relative to the unit cell of nitrogen atoms,[26] using the lattice parameter dependences given in Ref. 28.

573 K: $pO_2 \approx 10^{-24}$ Pa; at 673 K: $pO_2 \approx 10^{-18}$ Pa), the oxide layer is constituted of an Fe_3O_4 sublayer adjacent to ferrite and an α-Fe_2O_3 sublayer at the surface in direct contact with the oxidizing atmosphere. In the present work it was observed that α-Fe_2O_3 formed in an early stage of oxidation of α-Fe and that Fe_3O_4 developed on prolonged oxidation (see Figs. 9a and 10a). Thermodynamically the development of Fe_3O_4 is favored if only the chemical Gibbs-free energies (per mole O_2) are considered. It is suggested that a direct nucleation of hematite, instead of magnetite, is favored on ferrite covered by a Nital-etch promoted, (hydr)oxide layer. This interpretation is consistent with results of a recent HREM investigation of iron-oxide layers[13] formed during oxidation, for 16 min at 573 K in pure O_2 at 1 atm, of, respectively, Nital-etched and atomically clean polycrystalline, pure-iron samples,

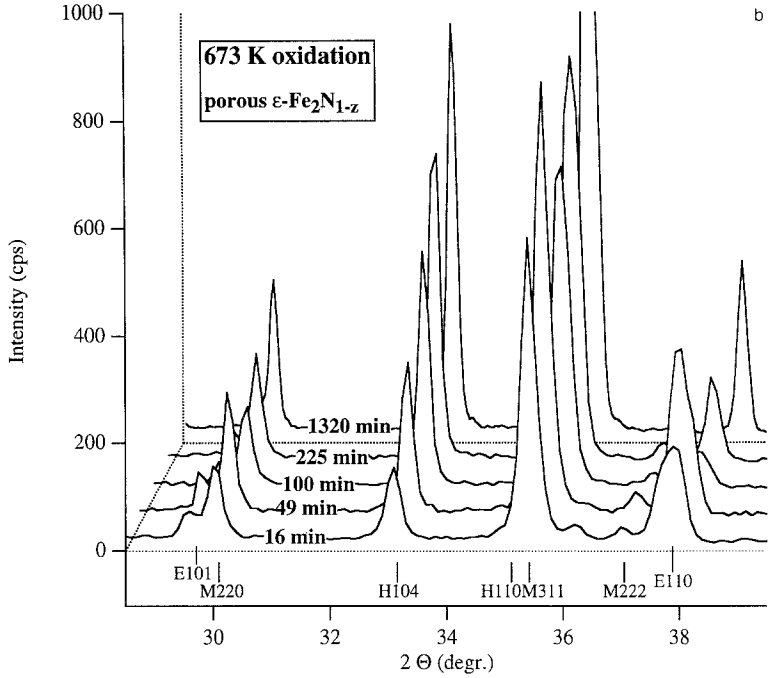

Fig. 10. Continued.

which yielded the following result. On the Nital-etched sample a thin oxide layer consisting of tiny crystallites of predominantly α-Fe_2O_3 developed; a minor amount of Fe_3O_4 was also present. Crystallites of both oxides were directly adjacent to the iron substrate. On the clean sample a relatively thick oxide layer consisting predominantly of Fe_3O_4 developed; if α-Fe_2O_3 was present, it occurred on top of Fe_3O_4. A similar initial nucleation of α-Fe_2O_3 as preferred over Fe_3O_4 in the temperature range 533–743 K can be deduced from the results given in Ref. 14.[¶]

It is anticipated that the nucleation of magnetite in the oxide layer as observed in an advanced stage of oxidation takes place at the α-Fe/α-Fe_2O_3 interface formed earlier. This may be consistent with the observation that the preparation procedure of α-Fe prior to oxidation influences the incubation time for the development of Fe_3O_4 in the oxide layer (cf. Fig. 9a, Oxide-Phase Development section and the results obtained in Ref. 13 as discussed above).

Using the above interpretation and results on initial oxidation of α-Fe at room temperature,[15,16] the observed kinetics of oxidation of α-Fe (Figs.

[¶]The oxidation times pertaining to the data in the figures of Ref. 14 are 5–10 times as long as in the present study; the partial pressure of oxygen was about 40 times as low.

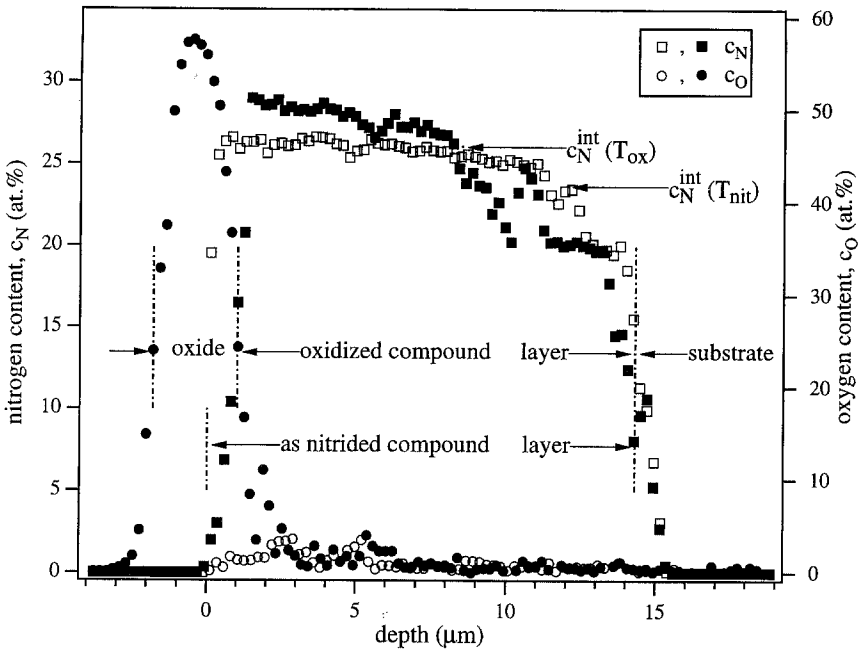

Fig. 11. Composition-depth profiles as determined with Electron Probe X-ray Microanalysis in cross-sections of a nitrided sample and of an identically nitrided and subsequently oxidized sample. Nitriding of α-Fe (Ferrovac-E) was performed in a gas mixture composed of 55 vol.% NH_3 and 45 vol.% H_2 at 838 K for $3\frac{1}{2}$ hr. Oxidation was performed in O_2 at 1 atm at 673 K for 16 hr. The nitrogen contents expected in ε-Fe_2N_{1-z} at the ε/γ' interface for the case of local equilibrium have been indicated for the nitriding temperature by c_N^{int} (T_{nitr}), and for the oxidation temperature by c_N^{int} (T_{ox}). The compound layer/substrate interface of the nitrided and oxidized sample was taken at the same depth as the compound layer/substrate interface of the nitrided sample to enable comparison of the profiles. Open symbols denote the as-nitrided sample; filled symbols denote the nitrided and oxidized sample.

1 and 2) may be explained as follows. Oxide growth occurs by diffusion of iron cations from the substrate through the oxide layer to the surface. The rate of the relatively rapid (cf. Fig. 2) initial development of hematite can be controlled by cation diffusion which is enhanced by the electrostatic field established over the thickness of the oxide layer as a result of coupled transport of cations and electrons.[15–18] At the present, elevated-temperature, electron transport predominantly occurs by thermionic emission rather than by tunneling through the potential barrier of the oxide layer.[15] The contribution of an electrostatic field to enhanced cation transport vanishes for thicker oxide layers (10–100 nm[15–17]), leading to a decrease of the oxidation rate. Then, the oxidation rate becomes controlled by cation diffusion due to only the chemical-potential gradient of the cations over the oxide layer. At this stage no local equilibrium in the sense of the Fe–O phase diagram occurs

(yet) at the ferrite-substrate surface due to the absence of magnetite. Thus, the nucleation of Fe_3O_4 at the α-Fe/α-Fe_2O_3 interface can be ascribed to a driving force for establishing local equilibrium at all phase interfaces in the iron/oxide layer assembly. Then, if a continuous Fe_3O_4 sublayer has formed between the α-Fe_2O_3 sublayer and α-Fe and, in view of the (now constant) boundary conditions for layer growth, diffusion-controlled layer growth can occur. Parabolic layer-growth kinetics, as observed after about 100 min at 673 K (see Fig. 2), for a dual phase oxide layer can occur if diffusion of the same species, in the present case iron cations, is rate-determining in both sublayers and if the boundary conditions for solving Fick's second law can be expressed in terms of $x/\sqrt{t}$, with x as the position coordinate for one-dimensional diffusion and t as the time.[19]

The parabolic growth constant ($k_p = \partial(\Delta m/A)^2/\partial t$) at 673 K, in the region where parabolic mass increase occurs, is about the same for the three types of α-Fe used (Fig. 2): $k_p = 0.15$–$0.2\ \mu g^2/cm^4$ sec. This value agrees very well with experimental values for k_p given in Refs. 20 and 21 for the oxidation of Ferrovac-E at 673 K, and is about ten times larger than the maximal estimate for k_p that is obtained for the growth of an Fe_3O_4 layer on α-Fe taking bulk diffusion of cations through Fe_3O_4 at 673 K as rate limiting: $\sim 0.02\ \mu g^2/cm^4$ sec.[22] Furthermore, the presence of α-Fe_2O_3 on top of Fe_3O_4 would lead to a reduction of the value for k_p for the whole (i.e., composite) dual Fe_3O_4/α-Fe_2O_3 layer.[23] Therefore, it is concluded that transport of the growth-rate-determining species (cations) in the present experiments occurs largely via short circuits (e.g., grain boundaries).

A detailed interpretation of the oxidation behavior of α-Fe at 573 K on the basis of the present results is not possible. The magnitude of the mass changes observed (Fig. 1) is comparable to the instrumental drift (cf. Thermogravimetric Analysis (TGA) section).

From the results in Figs. 3, 9a and 10a it is observed that the oxidation stage where blister formation occurs coincides with the stage where magnetite develops at the hematite/ferrite interface. The mechanism for blister formation is discussed in relation to the development of residual strains in the oxides in the following paper.[9]

Oxidation Kinetics of ε-Fe_2N_{1-z}

In contrast with the oxidation of α-Fe, oxide-layer development on ε-Fe_2N_{1-z} appears to start with the nucleation of Fe_3O_4, followed by the development of α-Fe_2O_3. This observation is consistent with results obtained earlier for the formation of an oxide layer on γ'-Fe_4N_{1-x} (at 603 K), where an incubation time for hematite nucleation was observed, whereas magnetite had nucleated in an earlier stage of oxidation.[7]

The oxidation rate of ε-Fe_2N_{1-z} (in terms of mass increase) seems to be faster initially than the oxidation rate of α-Fe, irrespective of the temperature (Figs. 1 and 2). Further, an increase of the nitriding time for otherwise identical nitriding conditions resulted in an even stronger initial uptake of oxygen (compare oxidation curves for ε-Fe_2N_{1-z} layers obtained after 3, $3\frac{1}{2}$, and 4 hr of nitriding at 838 K in Fig. 1). This influence of the nitriding time on the initial oxygen uptake indicates that the initial relatively fast uptake of oxygen can be explained, at least partly, as the result of porosity in the surface part of the layer; the extent of porosity and thereby the total surface area of ε-Fe_2N_{1-z} in immediate contact with the gaseous environment increases with nitriding time (pores develop by N_2 formation; pores coalesce to channels).[10] Hence, initially a larger effective surface area for oxygen uptake is offered by ε-Fe_2N_{1-z} than by α-Fe, which effect is the larger the longer the nitriding time.

At 573 K the initial difference in oxidation rate between ε-Fe_2N_{1-z} and α-Fe is reduced significantly on prolonged oxidation. In view of the above discussion the strong reduction of the oxidation rate of the ε-Fe_2N_{1-z} substrate is attributed to isolation of (part of) the large inner surface area (channel/pore walls) from the outer O_2 atmosphere by an oxide layer at the specimen surface. Although the largest part of the discrepancy in oxidation rates then is eliminated, the oxidation rates for α-Fe and ε-Fe_2N_{1-z} do not become equal because of different phase constitutions of the respective oxide layers on these substrates. For α-Fe upon oxidation at 573 K no continuous layer of magnetite has developed yet between the hematite layer and the substrate (see Oxidation Kinetics of α-Fe section), while magnetite is present on the iron-nitride layer. The growth of magnetite between hematite and the substrate may have a growth-rate enhancing effect (see below).

At 673 K the initial difference in oxidation rate between ε-Fe_2N_{1-z} and α-Fe has disappeared almost entirely after approximately 100 min of oxidation. This suggests that at this stage of oxidation the oxide layer on ε-Fe_2N_{1-z} has isolated the porous region inside the ε iron nitride from the gas atmosphere and that the phase constitutions of the oxide layers on α-Fe and on ε-Fe_2N_{1-z} are similar. The slower growth rate of the oxide layer on ferrite for times shorter than about 100 min may be related to the absence of magnetite between hematite and the substrate in this stage (see above).

Porosity in the nitride at the oxide/nitride interface may develop partly during oxidation as well. The incorporation of an iron cation into the oxide layer leaves behind an iron vacancy at the nitride side of the iron-oxide/nitride interface. The condensation of various iron vacancies in the substrate can lead to the development of voids near the oxide/nitride interface. It is noted that such sites may act as energetically favorable sites for the combination of nitrogen, dissolved in the ε phase, to N_2,[8] which process is promoted

by the local increase of the nitrogen content in ε-nitride close to the oxide/nitride interface, because of the withdrawal of iron atoms for oxide formation (see Fig. 11 and the following section).

Redistribution of Nitrogen in the ε-Fe_2N_{1-z} Sublayer During Oxidation

The composition range of the ε-Fe_2N_{1-z} sublayer of the nitride layer changes during oxidation. The nitrogen content in ε-Fe_2N_{1-z} at the oxide/ε-sublayer interface is higher than the initial nitrogen content at the surface of the as-nitrided layer; the nitrogen content at the ε-sublayer/γ'-sublayer interface is higher after oxidation than prior to oxidation (Fig. 11).

The local nitrogen accumulation at the nitride/oxide interface is ascribed to the withdrawal of iron atoms from the nitride layer for oxide formation at the outer surface. The same mechanism was taken responsible for the earlier observed occurrence of an ε-Fe_2N_{1-z} sublayer at the interface between γ' nitride and oxide.[7,8] Further, the overall higher nitrogen content after oxidation and the relatively smooth nitrogen-concentration depth profile in the ε-Fe_2N_{1-z} layer are attributed to diffusion of nitrogen to larger depth evoked by the enhancement of the nitrogen content at the oxide/nitride interface.

The observed increase of the nitrogen content in ε-nitride at the ε-sublayer/γ'-sublayer interface can be well understood in view of the Fe–N phase diagram[24,25]: oxidation implies annealing of the nitride layer at the oxidizing temperature. For comparison, the ε/γ' interfacial nitrogen contents in ε at the nitriding temperature and the oxidation temperature, assuming local equilibrium at this interface, have been indicated in Fig. 11. Consequently, ε-nitride with a relatively low nitrogen content (at the ε/γ'-interface) tends to decompose into ε-nitride with a relatively high nitrogen content and γ'-nitride. The re-establishment of local equilibrium at the ε/γ' interface during oxidation can be realized by contributions of the following processes:

(i) precipitation of γ'-nitride in the bottom region of the ε-nitride layer (see Figs. 6 and 11);
(ii) extension of the γ'-sublayer towards the surface at the cost of ε-nitride (see Fig. 11: ε/γ' interface is shifted towards the surface on oxidation);
(iii) supply of surplus nitrogen from the surface region of the ε-sublayer, by diffusion (see above).

Decomposition processes occurred in the γ' sublayer as well. The homogeneity range of γ'-nitride is smaller at the oxidation temperatures than at the nitriding temperature (see Fe-N phase diagram[24,25]: both the nitrogen

content at the ε/γ'-interface and the nitrogen content at the γ'/α-interface have to increase on oxidation. Precipitation of ferrite in the substrate-adjacent part of the γ'-layer may occur in association with an increase of the local nitrogen content of γ'-nitride, as observed (cf. Morphology section and Ref. 7). This implies that supply of nitrogen from the surface region by diffusion is not sufficiently rapid to realize the higher equilibrium nitrogen content in γ'.[7]

CONCLUSIONS

During oxidation of α-Fe at 573 K and 673 K in O_2 at 1 atm first α-Fe_2O_3 nucleates and later Fe_3O_4 develops. The development of magnetite between hematite and the iron-supplying substrate enhances oxide-layer growth kinetics. During oxidation of ε-Fe_2N_{1-z} under identical conditions the oxide phases appear in reverse order. Initially, the oxygen uptake is much faster for ε-Fe_2N_{1-z} than for α-Fe, because ε-Fe_2N_{1-z}, as prepared by nitriding of α-Fe, is porous and offers a much larger effective surface area for oxygen uptake. The oxidation rates of α-Fe and ε-Fe_2N_{1-z} become equal if the oxide layer on ε-Fe_2N_{1-z} isolates the porous region inside the ε iron nitride and if the constitutions of the oxide layers on α-Fe and ε-Fe_2N_{1-z} have become similar (i.e., α-Fe_2O_3 and Fe_3O_4 layers are present). This occurs after about 50 min of oxidation at 673 K and does not occur at 573 K until at least 1000 min of oxidation. The parabolic growth constants observed at 673 K after about 100 min suggest that oxide layer growth on both α-Fe and ε-Fe_2N_{1-z} is rate controlled by short circuit diffusion of the iron cations.

Concurrent with the appearance of magnetite in the oxide layer on α-Fe blister formation was observed. No blister formation occurred for the oxide layer on ε-Fe_2N_{1-z}.

An increase of the nitrogen content in the nitride at the nitride/oxide interface occurs during oxidation due to the withdrawal of iron atoms from the nitride for oxide formation at the outer surface. During oxidation precipitation processes occur in the ε and the γ' iron-nitride layers in association with changes of the nitrogen contents close to the interfaces of the nitride sublayers. These observations can be understood on the basis of the Fe–N phase diagram.

ACKNOWLEDGMENTS

The authors are grateful to Ing. N. Geerlofs, A. W. J. Gommers, and B. Sprong for provision and operation of the thermobalance, nitriding, and oxidation furnaces. P. F. Colijn assisted with light-optical microscopy. We

are obliged to Ir A. Buis of the Faculty of Aerospace Engineering for providing SEM facilities. We thank Dr. Th. H. de Keijser and Ing. N. M. van der Pers for the provision of X-ray diffraction facilities. Dr. W. G. Sloof and J. Helmig performed the EPMA measurements. These investigations have been supported financially by the Foundation for Fundamental Research of Matter (FOM), the Netherlands Technology Foundation (STW), and IOP-Metalen.

REFERENCES

1. K. Sachs and D. B. Clayton, *Heat Treat. Met.* **6**, 29 (1979).
2. B. De Benedetti and E. Angelini in *Advances in Surface Treatments* **5**, (1987), Niku-Lari, ed. (Pergamon Press, Oxford), pp. 3–11.
3. "Metals Handbook", Ninth Edition, Vol. 4, (American Society for Metals, Metals Park, Ohio, 1978), pp. 191–221.
4. G. Wahl, *Fachber. Hüttenpraxis Metallweiterverarb.* **19**, 1076 (1981).
5. C. Dawes and D. F. Tranter, *Heat Treat. Met.* **12**, 70 (1985).
6. *TF1-AB1 (QPQ) of Degussa-Durferrit, Sursulf-Oxynit of Hydromechanique et Frottement and Nitrotec S of Lucas.*
7. M. A. J. Somers and E. J. Mittemeijer, *Metall. Trans.* **21A**, 901 (1990).
8. M. A. J. Somers, B. J. Kooi, W. G. Sloof, and E. J. Mittemeijer, *Surf. Interface Anal.* **19**, 633 (1992).
9. B. J. Kooi, M. A. J. Somers, R. Jutte, and E. J. Mittemeijer, *Oxid. Met.* **48**, 111 (1997).
10. M. A. J. Somers, E. J. Mittemeijer, *Surf. Engng.* **3**, 123 (1987).
11. G. F. Bastin and H. J. M. Heijligers, *Scanning* **12**, 225 (1990).
12. H. A. Wriedt, *Binary Alloy Phase Diagrams*, Vol. 2, T. B. Massalski, ed. (American Society for Metals, Materials Park, Ohio, 1990), pp. 1739–1744.
13. P. C. J. Graat, M. P. H. Brongers, H. W. Zandbergen, M. A. J. Somers, and E. J. Mittemeijer, *Microscopy of Oxidation, Vol.* 3 (The Institute of Materials, London, 1997) pp. 493–504.
14. E. J. Caule, K. H. Buob, and M. Cohen, *J. Electrochem. Soc.* **108**, 829 (1961).
15. P. C. J. Graat, M. A. J. Somers, A. M. Vredenberg, and E. J. Mittemeijer, submitted for publication in *J. Appl. Phys.*
16. B. J. Kooi, M. A. J. Somers, and E. J. Mittemeijer, *Thin Solid Films* **281**, 488 (1996).
17. A. T. Fromhold and E. L. Cook, *Phys. Rev.* **163**, 650 (1967).
18. W. W. Schmeltzer and D. J. Young, *Progress in Solid-State Chemistry* **10**, 17 (1975).
19. M. A. J. Somers and E. J. Mittemeijer, *Metall. Mat. Trans.* **26A**, 57 (1995).
20. D. Caplan and M. Cohen, *Corros. Sci.* **6**, 321 (1966).
21. M. J. Graham and M. Cohen, *J. Electrochem. Soc.* **116**, 1430 (1969).
22. A. Atkinson, M. L. O'Dwyer, and R. I. Taylor, *J. Mat. Sci.* **18**, 2371 (1983).
23. A. Atkinson, *Diffusion Phenomena in Thin and Microelectronic Materials*, D. Gupta and P. S. Ho, eds. (Noyes Publications, New Jersey, 1988), pp. 204–244.
24. H. A. Wriedt, N. A. Gokcen, and R. H. Nafziger, *Binary Alloy Phase Diagrams*, Vol. 2, T. B. Massalski, ed. (American Society for Metals, Materials Park, Ohio, 1990), pp. 1728–1730.
25. B. J. Kooi, M. A. J. Somers, and E. J. Mittemeijer, *Metall. Mater. Trans.* **27A** 1063 (1996).
26. K. H. Jack, *Acta Cryst.* **5**, 404 (1952).
27. R. Delhez, Th. H. de Keijser, and E. J. Mittemeijer, *Surf. Engng.* **3**, 331 (1987).
28. M. A. J. Somers, B. J. Kooi, L. Maldzinski, E. J. Mittemeijer, A. A. van der Horst, A. M. van der Kraan, and N. M. van der Pers, *Acta Mater.* in press.